

Structure-property relationships of sheared carbon black suspensions determined by simultaneous rheological and neutron scattering measurements

Julie B. Hipp,¹ Jeffrey J. Richards,^{1,2,a)} and Norman J. Wagner^{1,b)}

¹Center for Neutron Science, Department of Chemical and Biomolecular Engineering, University of Delaware, Newark, Delaware 19716

²NIST Center for Neutron Research, National Institute of Standards and Technology, Gaithersburg, Maryland 20899

(Received 20 October 2018; final revision received 24 February 2019; published 9 April 2019)

Abstract

Carbon black suspensions exhibit complex, shear-dependent macroscopic properties that are a consequence of the state of the suspension microstructure. In this work, the shear-induced microstructure of a model, reversible suspension of conductive carbon black in propylene carbonate is measured using simultaneous steady shear rheology and small angle neutron scattering. These experiments provide microstructural evidence for a bifurcation in the rheological properties. We show that the demarcation line for this bifurcation is the inverse Bingham number, Bi^{-1} , which relates the magnitude of the stress response to an applied shear rate to the yield stress of the presheared suspension. At high shear rates where $Bi^{-1} > 1$, the suspension flows homogeneously and exhibits a thixotropic response that arises due to the self-similar breakdown of agglomerates with increasing shear rate. Conversely, at low shear rates where $Bi^{-1} < 1$, the applied shear drives the densification and growth of these agglomerates. This densification process leads to a gravitationally driven instability resulting in an inhomogeneous volume fraction distribution along the height of the geometry that is a function of both time under shear and shear rate. Under these shear conditions, the suspension exhibits apparent rheopexy, or antithixotropy, where a significant decline in the viscosity is observed with a step down in shear rate. The unique microstructural measurements presented here reconcile many observations in the literature regarding carbon black suspensions, including an apparent shear-thickening behavior, tunability of both the yield stress and elasticity through shear history, and transient macroscopic properties. © 2019 The Society of Rheology. <https://doi.org/10.1122/1.5071470>

I. INTRODUCTION

The behavior of colloidal suspensions under flow plays an important role in applications ranging from foodstuffs and personal care products to cements and paints [1–3]. When suspended, colloidal particles often exhibit attractive interactions comparable to their thermal motion, where the relative magnitude of the attraction determines the macroscopic properties of the suspension [4,5]. While significant effort has been dedicated to understanding the properties of homogeneous suspensions with weak attractions [6,7], the behavior of suspensions with strong attractions is less understood and is often complicated by heterogeneities associated with phase separation or sedimentation. In suspensions with strong, long-range interparticle attractions, phase instabilities exist at extremely low volume fractions such that a stable fluid phase may not exist at relevant particle loadings. Under these conditions, there is no well-defined equilibrium state and the properties of the suspension become linked to the distribution of floc sizes within the suspension. These flocs can be restructured by the flow, which in turn affects the macroscopic properties of the suspension [8–11]. This restructuring process can manifest itself in a variety of ways including

structural degradation [12–15], structural densification [16,17], and flow-induced anisotropy [18–22]. While it is generally assumed that this restructuring process dictates the macroscopic properties of the suspension, direct measurements of the presumed structure-property relationships and the effects of shear history are necessary, but often lacking, for improving the formulation and processing of colloidal suspensions for a broad range of applications.

Carbon black suspensions are a highly relevant example of thixotropic colloidal suspensions as they are used in numerous technological applications ranging from inks and tire rubbers to electrochemical energy storage devices [23–26]. Key design parameters in these applications include particle-matrix compatibility, suspension viscosity, and the electrical conductivity of the suspension. These properties depend on the microstructure and are subject to change depending on the shear history. It has been widely reported that carbon black suspensions tend to form stable gels with a finite yield stress and elasticity at intermediate weight fractions of a few percent solids [5,27]. Upon cessation of shear, these gels recover quickly and exhibit quiescent properties, such as a yield stress and conductivity, that depend on the flow history [28,29]. For example, a “tunable yield stress” that increases with increasing preshear intensity has been observed by Ovarlez *et al.* for a suspension of carbon black in mineral oil. This was attributed to an increase in the degree of jamming with increasing shear intensity [28]. When shear is applied, these suspensions flow with a shear-

^{a)}Present address: Department of Chemical and Biological Engineering, Northwestern University, Evanston, IL 60208.

^{b)}Author to whom correspondence should be addressed; electronic mail: wagnernj@udel.edu

thinning behavior that is consistent with structural breakdown of the carbon black agglomerates present within the suspension. This breakdown process has been widely accepted as a thixotropic process, where a time-dependent microstructural transition leads to a transient increase in viscosity with decreasing shear intensity [30–32]. However, for suspensions of carbon black in a mineral oil and tetradecane blend, Negi and Osuji have shown that at shear conditions near a critical stress, the viscosity undergoes an apparent shear-thickening transition [33]. Additionally, for a suspension of carbon black in an ethylene carbonate and dimethyl carbonate blend, Narayanan *et al.* have shown a similar thickening behavior where an increase in preshear intensity leads to an increase in the intrinsic flow curve viscosity [34]. Simultaneous optical and rheological measurements performed by Osuji *et al.* on carbon black in tetradecane show that at low shear rates, a loosely connected network of dense flocs is formed, which then transforms into a dense network of finely dispersed agglomerates at shear rates above the shear-thickening transition [35]. This structural transformation suggests that this apparent shear-thickening transition arises due to a change in hydrodynamic volume fraction between low and high shear rates [19,33,35]. This microstructural transition is rheopectic, or antithixotropic, such that a time-dependent decrease in viscosity is measured with a step down in shear rate [28,29]. Furthermore, for carbon black suspended in mineral oil, Helal *et al.* have observed a significantly lower conductivity and yield stress plateau when performing flow cessations over longer periods of time [29]. This transient behavior was attributed to a microstructural evolution at low shear intensities, such that weaker, less conductive gels are formed by shearing at low intensities for longer times [29].

Despite these observations and many related studies aimed at understanding the macroscopic properties of carbon black suspensions under flow, measurements of the purported microstructural basis for this shear-induced behavior remain largely a matter of conjecture. To resolve this, we directly measure structure-property relationships in such suspensions by performing a series of *in situ* Rheo-small angle neutron scattering (Rheo-SANS) experiments on a model carbon black suspension that exhibits an apparent shear-thickening behavior, a tunable yield stress, and transient macroscopic properties. These experiments are twofold: Rheo-uSANS experiments were performed to thoroughly characterize the quasisteady state microstructure of the suspension over a broad range of applied shear rates, and spatiotemporally resolved Rheo-SANS measurements were performed to investigate the local volume fraction distribution of carbon black as a function of Couette height, shear rate, and shear time. Results from these experiments enable the development of a quantitative understanding of the complex effect of shear-induced microstructural rearrangements on the time-dependent rheological behavior of these suspensions. Complementary rheo-electric measurements performed in a custom designed smooth-wall Couette and rheological tests performed in a rough-wall Couette further confirm our microstructural characterization. From these measurements, we identify two shear-dependent microstructural trajectories that are demarcated by the inverse Bingham number, Bi^{-1} .

Results from these experiments not only validate previous observations about the shear-induced structure of carbon black suspensions, but also show that under certain conditions, these suspensions exhibit concentration gradients driven by sedimentation, which further contribute to the apparent macroscopic properties.

II. MATERIALS AND METHODS

A. Sample preparation

The carbon black used in this study is Vulcan XC-72 (Cabot Corporation). The hierarchical structure of this high-structured conductive carbon black consists of porous, spherical primary particles with $R_{pp} = 20$ nm. These primary particles are fused together to form fractal primary aggregates with a hydrodynamic radius of $R_H = 135$ nm and a fractal dimension of $D_f = 2.7$ [27]. Suspensions of Vulcan XC-72 in neat propylene carbonate exhibit long-range attractions and short range repulsions, where the Hamaker constant is expected to be roughly $27 k_B T$ and the zeta potential is measured as $\zeta = -20$ mV [27,36]. As the volume fraction is increased, these primary aggregates form micrometer-sized agglomerates in suspension which eventually grow in size and jam to form a system spanning network at $\phi_{eff} = 0.23$ [27]. Previous neutron scattering and dynamic light scattering measurements confirm that in dilute suspension Vulcan XC-72 is colloidally stable with a well-characterized hydrodynamic size [27]. The suspension was prepared in the gel phase at $\phi_{eff} = 0.274$ (8.0 wt%, $\phi_{CB} = 0.056$) of Vulcan XC-72 carbon black in propylene carbonate (Acros, $\eta_m = 0.0026$ Pa s, dielectric constant, $\epsilon = 64$, $\rho = 1.204$ g cm $^{-3}$) using a Silverson L4RT high-shear homogenizer with a square hole high-shear screen set at 7000 rpm (733 rad/s) for 10 min. This high-shear homogenization is similar to what has been implemented previously by Dullaert and Mewis with the purpose of fully dispersing carbon black particles in a similar suspension, leading to a reversible, thixotropic dispersion [37].

B. Rheological measurements

The carbon black suspension was rehomogenized for 5 min prior to loading into the rheometer. All rheological measurements were prefaced with a conditioning step where twenty 30 s flow ramps from 500 to 0.1 s $^{-1}$ were performed followed by a waiting period of 20 min. After this waiting period, the material was sheared at a shear rate of 2500 s $^{-1}$ until a steady stress was achieved. This conditioning protocol was designed to erase any structural memory of the high-shear homogenization protocol and remove effects of sample loading. Rheological characterization was performed using a TA Instruments DHR-3 stress-controlled rheometer with a 42 mm long sandblasted Couette geometry [outer diameter (OD) = 30 mm, inner diameter (ID) = 28 mm, truncation gap = 6 mm]. Experiments were performed by applying a 600 s preshear at 2500 s $^{-1}$ to return the suspension to a similar structural state prior to each measurement, followed by a long shear step for 2000 s where the transient material response was recorded.

The yield stress of the presheared suspension was determined by performing creep experiments. In this protocol, the response of the suspension was probed under applied stress values in 5 Pa increments from 70 to 110 Pa. Prior to each applied stress, the suspension was sheared at 2500 s^{-1} for 600 s and allowed to rest for 60 s. This preshear step was used to rejuvenate the sample between each step so that both the stress and the structure returned to the same state prior to each applied shear stress. The yielding behavior is time dependent and depending on the time window chosen for the measurement, the value of the yield stress may change [38,39]. Our presheared suspension exhibits a yield stress between 70 and 90 Pa (Fig. S.1 [63]). Further creep experiments were performed using a similar protocol with different preshear shear rates.

C. Rheo-electric measurements

Simultaneous steady shear rheology and impedance spectroscopy measurements were performed using an ARES G2 strain-controlled rheometer equipped with a 34 mm long custom built Couette geometry (OD = 27 mm, ID = 26 mm, truncation gap = 0.05 mm) [40,41]. The electrical properties of the suspension under shear were probed in the shear gradient direction, between the walls of the cup and bob. The impedance spectroscopy measurements were made using an Agilent 4980A LCR meter by performing logarithmically spaced frequency sweeps from 20 Hz to 2 MHz. The impedance magnitude and phase shift measured from the test were corrected for open and short circuit calibrations, and a standard salt solution was used to determine the cell constant of the Couette. Typical measurements are shown in Fig. S.3 [63]. At low frequencies, the response is dominated by electrode polarization, which arises due to ion buildup at the electrode/electrolyte interface. At higher frequencies, the effect of electrode polarization is minimized and the response represents contributions from both ionic and electronic charge carriers. Therefore, to evaluate the conductivity of the suspension under shear, a moderate frequency of $f = 20 \text{ kHz}$ was chosen [27]. These experiments were performed using identical protocols as those used in determining the steady shear behavior on the DHR-3 rheometer.

D. Rheo-uSANS measurements

Ultra small angle neutron scattering (uSANS) measurements were performed on the BT5 instrument at the NIST Center for Neutron Research in Gaithersburg, MD, USA [42]. The experiment utilized five buffers to measure the full q -range from $1 \times 10^{-3} > q > 3 \times 10^{-5} \text{ \AA}^{-1}$, where $q = 4\pi/\lambda \sin(\theta/2)$ with $\lambda = 2.4 \text{ \AA}$ and $\Delta\lambda/\lambda = 6\%$. Rheo-uSANS experiments were performed by positioning an Anton-Paar MCR-301 stress-controlled rheometer equipped with a quartz cup and 60 mm long titanium bob (OD = 29 mm, ID = 28 mm, truncation gap = 0.05 mm) between the monochromator and analyzer crystals in the neutron beam line and aligned in the flow-vorticity (1–3) plane. Thus, the reported scattering intensity is acquired with a scattering vector along the shear direction [43,44]. To increase the neutron flux, the uSANS instrument uses a vertical slit collimated neutron beam,

resulting in a high q -resolution in the horizontal direction and a lower q -resolution in the vertical direction. Therefore, the scattered intensity collected for a single slit smeared q -value has contributions from a wider q -range that is mainly determined by the vertical q -resolution of the uSANS instrument [42,45]. Due to this slit smearing, any evidence of shear-induced anisotropy in the scattering is masked [42,46,47]. The scattering data were reduced to absolute scale using standard procedures contained within the IGOR Pro reduction macros [45]. Data were fit to the Beaucage model [48,49] using the SASVIEW software package [50] to extract the shear rate dependence of the radius of gyration of carbon black agglomerates. Fits and detailed fit information are shown in Fig. S.4 and Table S.1 [63]. Prior to any tests, the conditioning protocol for steady shear rheological measurements was performed. Further rheological measurements were carried out in a similar manner as for the steady shear rheology measurements where a 2500 s^{-1} preshear step was followed by shearing at the selected shear rate for up to 1400 s, then sheared for roughly 10 000 s while structural data were measured. This preshear step rejuvenates the sample between each measured shear rate and allows for comparison across multiple measurements. The collected rheological data show small fluctuations that are not observed in other rheological data and are, therefore, attributed to instrumental effects from the specific rheometer and geometry used.

E. Spatiotemporally resolved Rheo-SANS measurements

Small angle neutron scattering (SANS) measurements were performed on the NG3 vSANS diffractometer at the NIST Center for Neutron Research in Gaithersburg, MD, USA. The measurements were performed over a q -range of $3 \times 10^{-1} > q > 1.4 \times 10^{-3} \text{ \AA}^{-1}$, with $\lambda = 6 \text{ \AA}$ and $\Delta\lambda/\lambda = 12\%$. Figure 1 shows a schematic of the experiment where an Anton-Paar MCR-501 stress-controlled rheometer equipped with a 36 mm long titanium Couette geometry (OD = 29 mm,

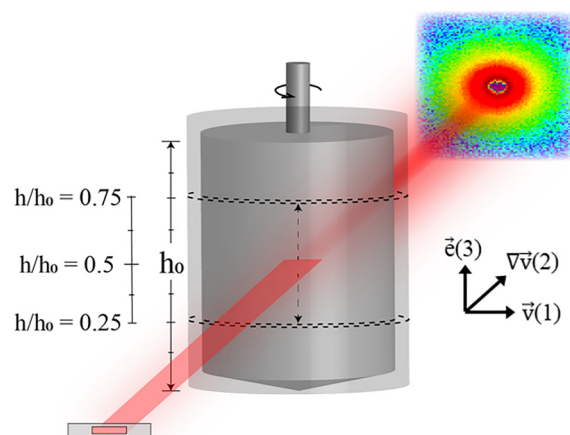


FIG. 1. Diagram of Rheo-SANS experiment where the Couette height is shown as $h_0 = 36 \text{ mm}$ and the measurable Couette region from $h/h_0 = 0.75$ to $h/h_0 = 0.25$ is highlighted. The incident beam is directed through the Couette geometry in the radial plane. Neutrons are transmitted through the Couette and are collected on a 2D detector as a scattering pattern.

ID = 28 mm, truncation gap = 0.09 mm) is positioned in the flow-vorticity (1–3) plane in the neutron beam line with a horizontal slit aperture of 1 mm tall by 5 mm wide. The length of the Couette is defined as $h_0 = 36$ mm and measurements performed at different heights along the Couette are defined as different values of h/h_0 . To perform discrete height scans, the rheometer was translated vertically to adjust the position of the rheometer with respect to the beam. Due to variations in thickness of titanium along the length of the bob (Fig. S.2 [63]), the measurable region for height scans was found to be between $h/h_0 = 0.25$ and $h/h_0 = 0.75$, such that the top and bottom 25% of the volume fraction profile in the geometry was not measured. During the height scans, scattering patterns were measured in 20 s increments at 10 discrete heights while the material was sheared at a steady rate. Accounting for the time required for vertical translation, each vertical scan was approximately 500 s long. These vertical scans from $h/h_0 = 0.75$ to $h/h_0 = 0.25$ were performed repeatedly for the duration of the run. This resulted in a total of 10 vertical scans and a measurement period of 5000 s for each shear rate. The scattering data were reduced to absolute scale using standard procedures and IGOR PRO reduction macros. *In situ* rheological measurements consisted of a 2500 s⁻¹ preshear step followed by a shear step at the selected shear rate for approximately 5000 s with height scans performed during both the preshear and steady shear steps.

The scattering measurements performed during the spatio-temporally resolved Rheo-SANS experiments are used to probe the structure of the carbon black suspension as a function of time, shear rate, and position along the Couette height. The measured scattering intensity, $I(q)$, is related to the structure of the suspension as follows [51,52]:

$$I(q) = \varphi(\Delta\rho)^2 V_p P(q) S(q) + I_b. \quad (1)$$

In Eq. (1), φ is the volume fraction of scattering objects in the beam, $\Delta\rho$ is the difference in scattering length densities between the two phases in the suspension, V_p is the volume of the primary carbon black aggregates, and I_b is the incoherent background. $P(q)$ is the form factor contribution to the scattering from immutable building blocks of the suspension, which in this case are the primary carbon black aggregates [27]. A fit to the form factor contribution is shown in Fig. 2(a). This form factor was found by measuring the scattering from a dilute suspension of Vulcan XC-72 in propylene carbonate and fitting to a modified Teixeira fractal model as described by Richards *et al.* [27]. $S(q)$ is the structure factor contribution to the scattering that arises due to interactions between primary aggregates. As shown in Fig. 2(a), the effect of the structure factor can be observed at low q and has no influence on the scattering at $q > 6 \times 10^{-3} \text{ \AA}^{-1}$ where the structure is described solely by the form factor, $P(q)$.

Equation (1) is interpreted to indicate that, in the absence of any changes in the microstructure, the effect of a change in φ due to sedimentation will be measurable at all q as a vertical shift in intensity. This change in φ can be quantified by calculating the scattering invariant, which requires an integration from $q = 0$ to $q = \text{infinity}$ [51,52]. However, it is also possible to isolate this volume fraction effect from any shear-induced structural changes and measure the extent of the sedimentation by examining the magnitude of the intensity at a q -range, where $S(q) \rightarrow 1$ [27]. These two analyses provide similar results, but due to the limited q -range of this measurement, the latter analysis is used here. The scattered intensity is observed to follow the form factor, $P(q)$, for $q > 6 \times 10^{-3} \text{ \AA}^{-1}$ [Fig. 2(a)]. Therefore, to examine and quantify changes in $I(q)$ due to changes in φ , the background subtracted intensity is integrated from $0.008 < q < 0.03 \text{ \AA}^{-1}$, where $S(q) \rightarrow 1$. This integral, I^* , is used to calculate a normalized volume fraction, $\hat{\varphi}_{\text{CB}}$, as follows:

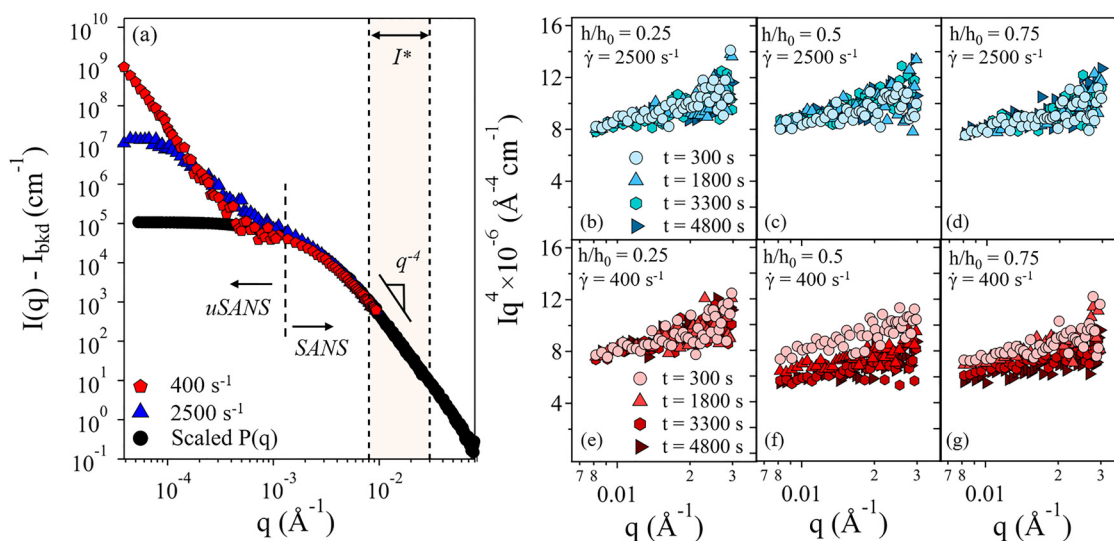


FIG. 2. (a) $I(q) - I_{\text{bkd}}$ plotted against q , summarizing a combination of Rheo-SANS and Rheo-uSANS experiments performed on a suspension of Vulcan XC-72 carbon black in propylene carbonate with $\varphi_{\text{eff}} = 0.274$. Pinhole smeared SANS measurements are shown with desmeared uSANS measurements. The primary aggregate form factor is shown in black circles. Shear-dependent scattering is shown from measurements at 2500 s^{-1} (blue triangles) and at 400 s^{-1} (red pentagons), and the q -range where $\hat{\varphi}_{\text{CB}}$ is measured is highlighted, (b)–(g) the progression of the background subtracted intensity in the highlighted region in (a) as $I(q) \times q^4$ plotted against q at different heights and times, where (b)–(d) are measured at 2500 s^{-1} and (e)–(g) at 400 s^{-1} .

$$\hat{\phi}_{\text{CB}} = \frac{I^*(h/h_0, t, \dot{\gamma})}{\langle I_{\text{preshear}}^*(\dot{\gamma}) \rangle}. \quad (2)$$

From Eq. (2), $\hat{\phi}_{\text{CB}}$ is the integral calculated at each height, time, and shear rate divided by the average integral calculated for the suspension during the preshear at all heights. In this way, $\hat{\phi}_{\text{CB}}$ is a measure of the relative change in carbon black volume fraction in the neutron beam with respect to the preshear distribution.

To illustrate the changes that occur due to sedimentation, a data set collected at different heights in the Couette and shear times for shear rates of 2500 s^{-1} and 400 s^{-1} are plotted in Figs. 2(b)–2(d) and Figs. 2(e)–2(g), respectively. The changes in background subtracted intensity that occur due to sedimentation are emphasized in the Porod plot of $I(q) * q^4$ vs q shown in Figs. 2(b)–2(g). In this q region, the intensity scales linearly with the volume fraction of dispersed phase particles [51,52]. These results show that at a high shear rate of 2500 s^{-1} , the volume fraction appears independent of shear time and height in the Couette. However, at a low shear rate of 400 s^{-1} , the volume fraction is a function of both the shear time and height, and further, the middle region of the Couette experiences a more significant change with time. Measurements such as those presented in Figs. 2(b)–2(g) were performed over a range of vertical positions in the Couette, shear rates, and time to determine sample heterogeneity.

III. RESULTS

A. Steady-state flow curve

The transient stress response over a broad range of applied shear rates is shown in Fig. 3(a), where a preshear of 2500 s^{-1} is applied to rejuvenate the sample before each

shear test. Two distinctly different transient stress responses are observed. For shear rates above 500 s^{-1} , the stress response exhibits an initial transient behavior that evolves to a quasisteady stress response after less than 500 s of steady shear. At shear rates of 250 s^{-1} and below, however, a large, transient stress decay is evident. Additionally, at shear rates below 250 s^{-1} , a steady stress is never fully achieved even after 2000 s of shearing.

The observed bifurcation in the rheological response of the suspension is characterized by plotting the stress and viscosity for each applied shear rate at different times throughout the flow start-up as presented in Figs. 3(b) and 3(c), respectively. For this presentation, three times were selected: 0 s, 500 s, and 1800 s. These times were chosen to emphasize rheological properties of the presheared suspension, the suspension after adjusting to the new applied shear rate, and the suspension at long times. The instantaneous stress response (red circles) shows an apparent yield stress plateau of 88 Pa at low shear rates, which is consistent with the range in yield stress between 70 and 90 Pa that was independently measured for the presheared suspension (Fig. S.1 [63]). Using this value of 88 Pa as the “true” yield stress of the presheared suspension, σ_y , a dimensionless group known as the inverse Bingham number, $Bi^{-1} = \sigma/\sigma_y$, is calculated. The inverse Bingham number is defined as the ratio of the measured or applied shear stress to the yield stress and is used to distinguish between the two flow regimes. To highlight the differences between the two flow regimes, Figs. 3(b) and 3(c) are plotted with closed symbols for points evaluated at $Bi^{-1} > 1$ and open symbols for points evaluated at $Bi^{-1} < 1$, where the apparent response is an averaged value over the entire Couette height.

From Fig. 3(b), it is apparent that the stress at $Bi^{-1} > 1$ does not change significantly in time and exhibits a similar power-law behavior with shear rate at all times evaluated. However, at low shear rates, where $Bi^{-1} < 1$, the apparent

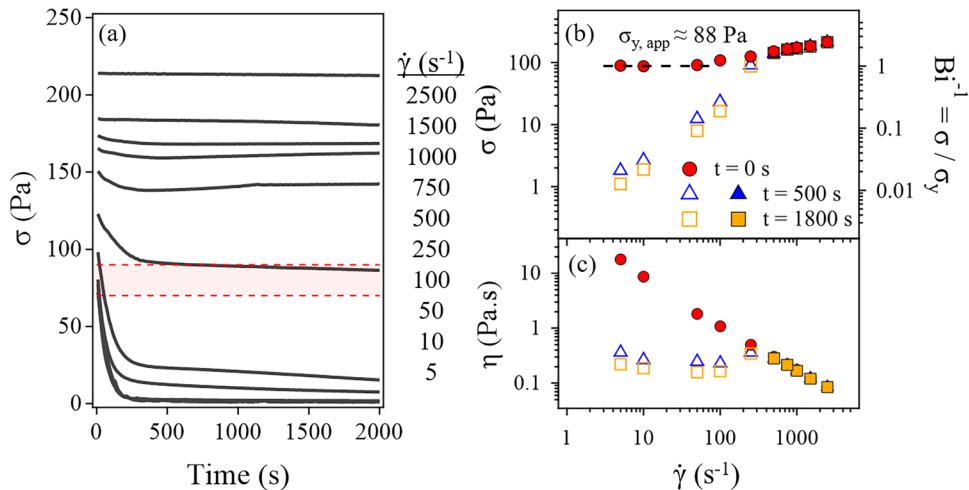


FIG. 3. (a) Time-dependent stress response measured after the standard preshear protocol for a range of shear rates from 2500 s^{-1} to 5 s^{-1} for a suspension of Vulcan XC-72 carbon black in propylene carbonate with $\phi_{\text{eff}} = 0.274$. The yield stress range measured in Fig. S.1 [63] is shown as a red highlighted region from 70 to 90 Pa. (b) Measured stress plotted against shear rate with the right axis shown as the inverse Bingham number, $Bi^{-1} = \sigma/\sigma_y$, and (c) viscosity plotted against shear rate extracted from the time-dependent stress shown in (a). The stress and viscosity at $t = 0 \text{ s}$ (red circles) were obtained by extrapolating the time-dependent stress response using an exponential fit. At low shear rates, the $t = 0 \text{ s}$ stress plateaus at an apparent yield stress of 88 Pa. The stress and viscosity is also plotted at 500 s (blue triangles) and 1800 s (yellow squares). Open and closed symbols are used to differentiate between values taken while the material is undergoing flow at Bi^{-1} less than and greater than 1, respectively.

stress decreases by over an order of magnitude in the first 500 s and continues to decrease at a slower rate throughout the measurement period. The transition between the two transient behaviors is notable in the flow curve and is consistent with the rheological behavior reported by Ovarlez *et al.* for a suspension of carbon black in mineral oil [28]. As presented in Fig. 3(c), an apparent shear-thickening transition similar to that observed by Osuji *et al.* [35] emerges at a shear rate of about 250 s^{-1} upon transitioning from shear conditions where $Bi^{-1} < 1$ to $Bi^{-1} > 1$. Additionally, an increase in the intensity of the shear-thickening transition is observed with longer shear times. Thus, our suspension exhibits many of the interesting, nontrivial shear-history dependent rheological behaviors reported in the literature.

B. A tunable yield stress

It has been observed for many thixotropic and rheopectic suspensions that the apparent yield stress of the suspension is tunable and is dependent on the flow history [28,29,53]. It is reported for these suspensions that both the time and intensity of the preshear are important in determining the macroscopic properties. To demonstrate the tunability of the apparent yield stress of this suspension, creep experiments were performed after a 600 s preshear at two shear rates, 1000 s^{-1} and 100 s^{-1} , or where $Bi^{-1} > 1$ and $Bi^{-1} < 1$, respectively, where the “true” yield stress of the suspension, $\sigma_y = 88 \text{ Pa}$ is used to calculate Bi^{-1} . After preshearing at 1000 s^{-1} , where the average stress response is 157 Pa ($Bi^{-1} = 1.8$), the suspension exhibits a transition from solid- to liquid-like behavior at applied stresses above 75 Pa , as seen in Fig. 4(a). This yielding transition occurs at stresses comparable to the yield stress of the presheared suspension (Fig. S.1 [63]). When the preshear is lowered to 100 s^{-1} , where the quasisteady stress response is 24 Pa ($Bi^{-1} = 0.3$), the yielding behavior occurs at applied stresses between 10 and 25 Pa as seen in Fig. 4(b). Therefore, the shear-history dependent yield stress measured after preshearing at a shear rate where $Bi^{-1} < 1$ is significantly lower than that measured at a shear rate where $Bi^{-1} > 1$. Regardless of the preshear intensity, the suspension is unable to undergo slow flow and

instead flows at high shear rates of 100 s^{-1} and greater. This behavior is a trademark of viscosity bifurcation and is consistent with observations by Ovarlez *et al.* for carbon black suspensions and is also commonly observed for other thixotropic suspensions [28,53].

C. Stress-conductivity connection

It has also been reported that the electrical properties of carbon black suspensions depend on both the intensity and duration of the applied shear [29,34,54,55]. To investigate this behavior and its relation to the microstructure of carbon black suspensions, rheo-electrical measurements were performed in both flow regimes using a custom-made Couette geometry [40,41]. Figure 5 shows the rheo-electric behavior measured after preshearing at 2500 s^{-1} for 600 s and stepping to shear rates of 2500 s^{-1} , where $Bi^{-1} > 1$ (black circles and lines) and 250 s^{-1} , where $Bi^{-1} < 1$ (red triangles and lines). The apparent stress response plotted as Bi^{-1} is shown as lines and the apparent conductivity, κ , measured at a frequency of $f = 20 \text{ kHz}$ is shown as symbols with dashed lines. For $Bi^{-1} > 1$, the suspension exhibits a constant conductivity and stress response in the entire measurement window, as was seen in the rheological data shown in Fig. 3(a). For $Bi^{-1} < 1$, however, both the apparent stress response and conductivity decrease by about an order of magnitude in the first 200 s of shearing and then transition to a more moderate decline that extends to long times. The similarity in the transience for the apparent stress and conductivity indicate that these two macroscopic properties are closely linked to one another, as was previously hypothesized for other suspensions of carbon black [29,34,54,55]. Helal *et al.* reported similar rheo-electric behavior by ramping from high to low shear stresses at different rates. In these experiments, it was shown that slower ramps lead to less conductive gels with lower viscosities [29]. This time-dependent behavior was also observed by Narayanan *et al.*, who measured a transient increase in resistance upon stepping down in shear rate [34]. These measurements provide indirect evidence for a transient microstructural evolution under shear, but a full understanding of this microstructural

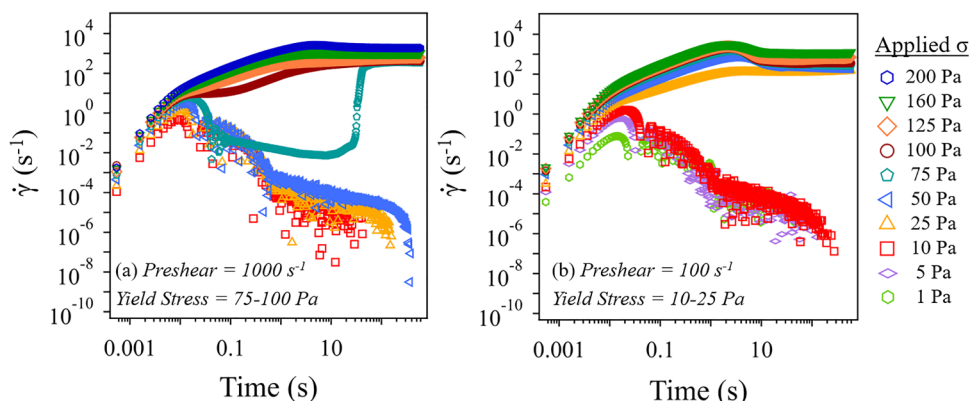


FIG. 4. Creep tests performed on a suspension of Vulcan XC-72 carbon black in propylene carbonate with $\phi_{\text{eff}} = 0.274$ after different preshear shear rates where the response to applied stresses ranging from 1 Pa to 200 Pa is plotted as shear rate against time, (a) response after 1000 s^{-1} preshear and (b) response after 100 s^{-1} preshear.

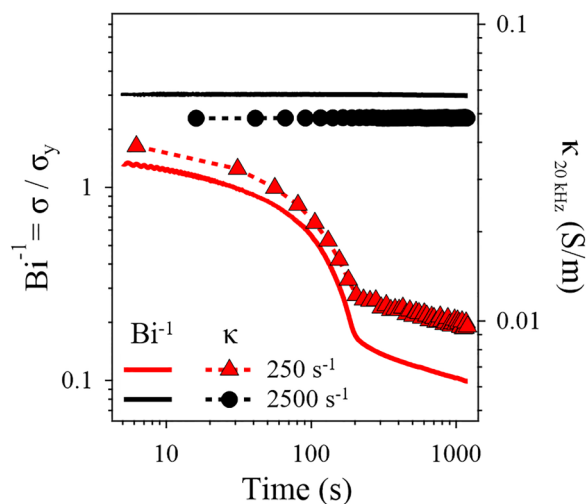


FIG. 5. Results from rheo-electric measurements performed on a suspension of Vulcan XC-72 carbon black in propylene carbonate with $\phi_{\text{eff}}=0.274$ in both flow regimes. Lines represent the transient stress plotted as Bi^{-1} and markers with dashed lines represent the conductivity measured at 20 kHz. Measurements were performed at applied shear rates of 2500 s^{-1} (black circles and lines) and 250 s^{-1} (red triangles and lines).

behavior and how it specifically influences the shear-history dependent macroscopic properties of the suspension requires *in situ* measurements, as discussed below.

D. Structural interrogation using Rheo-uSANS

To measure the microstructural origin of the observed macroscopic behavior and thus, establish structure-property relationships, Rheo-uSANS experiments were performed to directly evaluate the structural evolution of carbon black agglomerates under steady shear flow. As shown in Fig. 2(a), shear-induced structural changes occur at length scales that are accessible by uSANS experiments, but not SANS. In these experiments, the nontrivial link between the two observed trajectories in macroscopic behavior and the yield stress of the suspension was investigated by measuring the microstructure at a set of applied steady shear rates where $Bi^{-1} > 1$ and $Bi^{-1} < 1$.

1. Shear-induced structure at $Bi^{-1} > 1$

The stress response from a series of shear rates where $Bi^{-1} > 1$ is reported in Fig. 6(a). Consistent with the measured rheological behavior shown in Fig. 3(a), after a brief adjustment to a change in shear rate, the stress response is steady over the entire 4-h time window of the Rheo-uSANS measurement with small fluctuations that arise due to instrumental artifacts. The inset of Fig. 6(a) shows the steady shear viscosity, which exhibits a shear-thinning behavior where the viscosity scales with the shear rate as $\dot{\gamma}^{-0.74}$. The preshear response is shown at $t < 0 \text{ s}$ where the same stress value is reproducibly achieved before each shear rate measured, indicating that the same structure is achieved prior to each test. The dashed vertical line indicates the time of the start of the uSANS measurement.

Figure 6(b) shows the measured scattering intensity, $I(q)$, plotted against q measured at each shear rate in this range. It

has been established in prior work that attractive interactions between primary aggregates lead to phase instabilities in this suspension, which induce the formation of carbon black agglomerates [27]. These agglomerates are comprised of many primary aggregates that are joined together by intra-agglomerate associations. As shown in Fig. 6(b) by the systematic reduction in scattering intensity with increasing shear rate at low q , these intra-agglomerate associations break under shear, leading to an expected increase in the erosion of agglomerates with increasing shear rate [12–15]. The rate-independent scattering at higher q reflects the internal structure of these agglomerates, which is relatively open and unchanging with shear rate as observed by a constant power-law slope of about -1.9 between the scattering intensity and q at all shear rates. The scattering data shown in Fig. 6(b) were fit (Fig. S.4 and Table S.1 [63]) to extract a radius of gyration, R_g , of carbon black agglomerates at each shear rate in this flow regime [48,49]. The fitted values are plotted against the applied shear rate in the inset of Fig. 6(a) and show a scaling with shear rate as $\dot{\gamma}^{-0.26}$. By comparing the shear rate dependence of the viscosity and the radius of gyration, it is found that a relationship exists where the viscosity roughly scales as R_g^3 , as expected for systems dominated by hydrodynamic drag [8].

2. Shear-induced structure at $Bi^{-1} < 1$

The apparent stress response measured during Rheo-uSANS at shear rates for $Bi^{-1} < 1$ is reported in Fig. 7(a), where rheological behavior consistent with that shown in Fig. 3(a) is observed. Additionally, the apparent rheological response measured at 2500 s^{-1} from Fig. 6(a) is plotted for reference. These measurements show several abrupt increases in stress that are attributed to instrumental artifacts. Importantly, a steady shear stress is not achieved in these measurements. The vertical dashed lines in Fig. 7(a) mark the beginning of the uSANS measurement such that the scattering shown in Fig. 7(b) for $Bi^{-1} < 1$ is from quasisteady structures measured after the initial, rapid decline in apparent stress. Again, between each measured shear rate, a 2500 s^{-1} preshear successfully rejuvenates the sample to a nearly equivalent structural state. The transient apparent viscosity is plotted as an inset in Fig. 7(a) to show its evolution as a function of shear time and shear rate.

The shear-dependent scattering, plotted as open symbols in Fig. 7(b), shows a distinctly different behavior than what was measured at $Bi^{-1} > 1$, where the data for 2500 s^{-1} are reproduced from Fig. 6(b) for reference. Most evident is the significantly greater scattering intensity at low q with a strong power-law decay [$I(q) \sim q^{-3.6}$], which is indicative of surface scattering from large objects [56]. Thus, instead of the micrometer-sized agglomerates that form at $Bi^{-1} > 1$, the agglomerates formed at $Bi^{-1} < 1$ have sizes that exceed the q -range of the uSANS instrument ($>15 \mu\text{m}$). These agglomerates are more compact than those formed at $Bi^{-1} > 1$ as indicated by the decrease in intensity at higher q , which arises due to short range repulsions between primary aggregates. Similar structural growth accompanied by local densification processes have been observed previously by Rueb and Zukoski who used neutron scattering to measure the shear-dependent structure of octadecyl silica particles [16], by

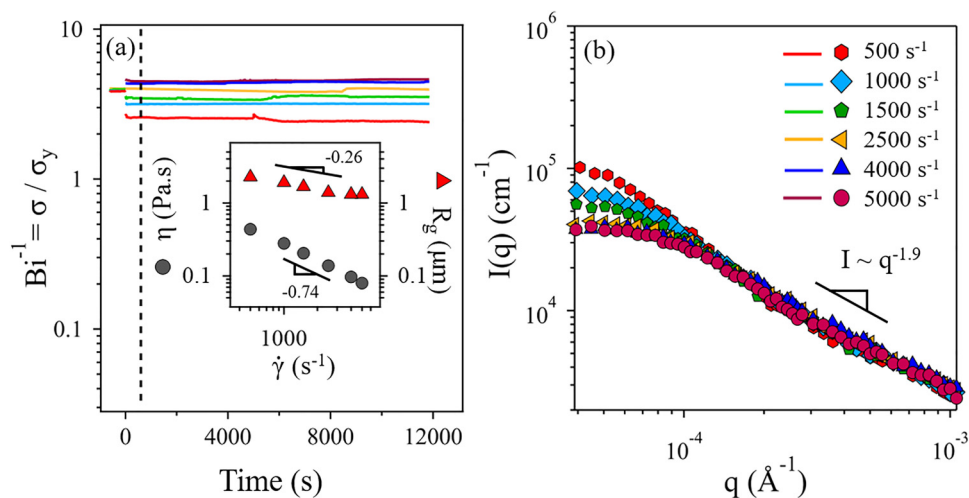


FIG. 6. Results from a Rheo-uSANS measurement performed at high shear rates on a suspension of Vulcan XC-72 carbon black in propylene carbonate with $\phi_{\text{eff}}=0.274$. (a) Time-dependent stress response measured during the Rheo-uSANS experiment plotted as Bi^{-1} . The region to the left of the dashed line shows the stress response to a 600 s preshear at 2500 s^{-1} and then a 600 s preshear at the shear rate measured. The region to the right of the dashed line shows the measured stress response during the uSANS measurement. Inset: measured viscosity and fitted radius of gyration plotted against shear rate. (b) Slit smeared scattering data shown as intensity, $I(q)$, plotted against q measured at different shear rates with the corresponding stress response shown in (a).

Koumakis *et al.* who performed rheo-confocal experiments on a colloid-polymer gel at low shear rates [57], and by Osuji *et al.* who imaged sheared carbon black suspensions [19,35]. These measurements, along with previous static measurements of suspensions of Vulcan XC-72 in propylene carbonate [27], provide further evidence for the formation of large-scale dense structures in the suspension. The slit smeared line scan inherent to the uSANS instrument precludes a more detailed analysis of the microstructure under these conditions, including detecting any shear-induced anisotropy.

In this flow regime, the suspension behaves rheopectically as indicated by over an order of magnitude decrease in the apparent viscosity upon stepping down in shear rate. This rheopectic behavior is driven by the densification and growth

of macroscopic agglomerates, which leads to expulsion of propylene carbonate from the internal volume of the agglomerates. This restructuring causes a decrease in the hydrodynamic volume fraction and a lower apparent viscosity despite the growing size of agglomerates. Therefore, it can be concluded that the decline in apparent stress that occurs prior to achieving a quasisteady state stress is directly related to the structural transformation from the loose, open agglomerates formed for $Bi^{-1} > 1$ to the large, dense agglomerates formed for $Bi^{-1} < 1$. Although the structures formed under these conditions appear to be relatively insensitive to shear rate, the transient apparent viscosity shows that the characteristic time of this restructuring process depends on the magnitude of the applied shear rate.

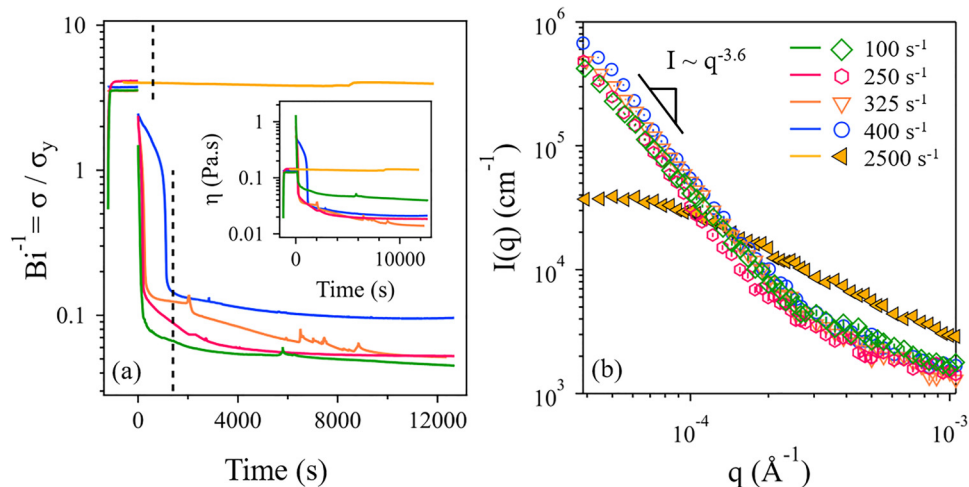


FIG. 7. Results from a Rheo-uSANS measurement performed at low shear rates on a suspension of Vulcan XC-72 carbon black in propylene carbonate with $\phi_{\text{eff}}=0.274$. (a) Time-dependent apparent stress response measured during the Rheo-uSANS experiment plotted as Bi^{-1} . The first 2600 s (left of the dashed line) show the apparent stress response to a 1200 s preshear at 2500 s^{-1} and then a 1400 s preshear at the shear rate measured. The apparent stress response to the right of the dashed line shows the apparent stress response during the uSANS measurement. Inset: apparent viscosity plotted against time measured during the Rheo-uSANS experiment. (b) Slit smeared scattering data shown as intensity, $I(q)$, plotted against q measured at different shear rates with the corresponding stress response shown in (a).

E. Investigating volume fraction heterogeneities using Rheo-SANS

Our steady shear measurements show that at applied shear rates such that $Bi^{-1} < 1$, the apparent stress response exhibits two behaviors. The first is observed at short times, where the stress decreases nearly an order of magnitude over relatively short time scales. Rheo-uSANS measurements show that this rapid decrease in stress is a signature of the densification and growth of agglomerates. The second behavior is the steady decline in stress observed after the initial restructuring period. It is known that sedimentation of non-Brownian particles can lead to an apparent shear-thinning behavior [58]. Therefore, it is likely that the apparent long-lived stress decline is due to sedimentation of the large, dense agglomerates formed at $Bi^{-1} < 1$. To investigate this, spatiotemporally resolved Rheo-SANS experiments were performed.

A heat map [Fig. 8(a)] of the volume fraction distribution in the Couette for a shear rate of 400 s^{-1} (i.e., where $Bi^{-1} < 1$) is plotted as $\hat{\varphi}_{CB}$ as a function of both the normalized height in the Couette, h/h_0 , and scan number such that each pixel corresponds to a $\hat{\varphi}_{CB}$ value measured at a specific height and time. The heat map is defined by the color legend shown on the right where the lowest value of $\hat{\varphi}_{CB}$ corresponds to a purple hue and the highest to a dark red hue. Averaged values for $\hat{\varphi}_{CB}$ were taken at $h/h_0 = 0.5$ (dashed line) at each scan and plotted with the apparent stress response as Bi^{-1} against time in Fig. 8(b). In Fig. 8(a), during the first 500 s long scan, the volume fraction distribution does not change significantly from the preshear distribution, while the apparent stress shown in Fig. 8(b) decreases significantly. After 500 s, the apparent stress continues to decline at a slower pace along with $\hat{\varphi}_{CB}$ at $h/h_0 = 0.5$. During this measurement, a carbon black lean region develops at $h/h_0 = 0.58$, which extends over a larger area of the Couette with prolonged shear.

The observed correspondence between the slow apparent stress decline at long times and the development of spatial

heterogeneities within the Couette height indicates that sedimentation plays an important role in the transient stress response. To emphasize the extent of sedimentation that occurs for $Bi^{-1} < 1$, a photograph has been provided as an inset in Fig. 8(b), which shows the Couette geometry several minutes after shear is stopped at the end of an experiment. This image shows a banded region near the middle of the Couette that contains no carbon black surrounded by two carbon black rich regions. This banded region is not observed while the suspension is under shear and develops after shear has stopped. Our results suggest that this apparent gel fracture is due to the depletion of carbon black in the center of the Couette so that the depleted region is unstable and falls to join the lower region, while the upper region remains pinned by the upper free surface.

To further examine the relationship between applied shear rate and sedimentation, similar heat maps were generated at all measured shear rates as shown in Fig. 9. As in Fig. 8(a), each panel is comprised of a series of pixels that each represent a value of $\hat{\varphi}_{CB}$ at a specific Couette height (y-axis) and scan number (x-axis). These experiments were performed in the same manner where each vertical scan is 500 s long and the entire measurement period is 5000 s long. The panels are divided into the two flow regimes where data measured at $Bi^{-1} < 1$ and $Bi^{-1} > 1$ are on the top and bottom row, respectively. At $Bi^{-1} < 1$, $\hat{\varphi}_{CB}$ is a strong function of the Couette height and shear time, as well as the applied shear rate. At 100 s^{-1} , a clear gradient develops from low to high $\hat{\varphi}_{CB}$ with decreasing Couette height. At shear rates from 250 to 500 s^{-1} , a carbon black lean region develops in the middle of the Couette as the particles move outside of the measurable window and presumably to the bottom 25% of the Couette. For $Bi^{-1} > 1$, $\hat{\varphi}_{CB}$ varies only slightly along the height of the Couette, but does not vary with shear time, indicating that the volume fraction distribution is stable. The relationship between the applied shear rate and the volume fraction distribution is complex and is dependent on several factors including the shear-induced microstructure and the ability for shear

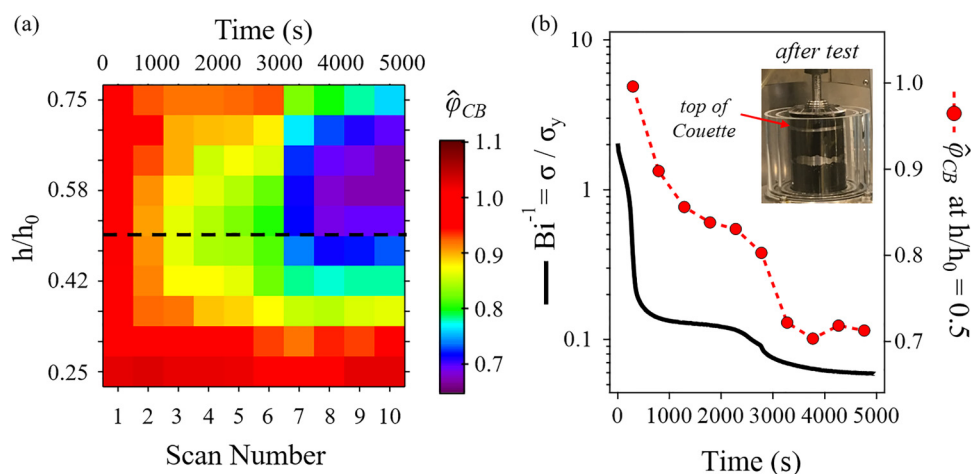


FIG. 8. Results from a Rheo-SANS measurement performed at 400 s^{-1} on a suspension of Vulcan XC-72 carbon black in propylene carbonate with $\varphi_{\text{eff}} = 0.274$. (a) $\hat{\varphi}_{CB}$ as a function of both the scan number and the normalized Couette height, h/h_0 (see Fig. 1). The legend on the right is used to depict different values of $\hat{\varphi}_{CB}$ where red corresponds to the highest $\hat{\varphi}_{CB}$ values and purple to the lowest $\hat{\varphi}_{CB}$ values. Each vertical scan lasts approximately 500 s. (b) The apparent stress response plotted as Bi^{-1} (black line) measured during the height scans and $\hat{\varphi}_{CB}$ measured at $h/h_0 = 0.5$ (red line and circles) plotted against measurement time. Inset: image of the suspension in the Couette geometry several minutes after shear is stopped.

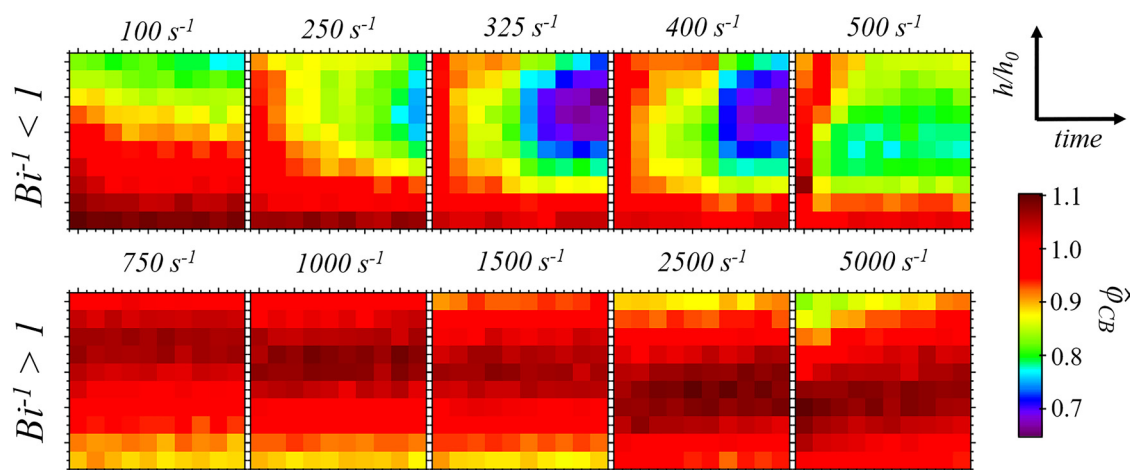


FIG. 9. Results from a Rheo-SANS measurement performed at ten shear rates on a suspension of Vulcan XC-72 carbon black in propylene carbonate with $\phi_{\text{eff}} = 0.274$. Each panel shows $\hat{\phi}_{\text{CB}}$ as a function of time and the normalized Couette height, h/h_0 , as shown by the coordinate system on the top right. The color legend on the bottom right is used to depict different values of $\hat{\phi}_{\text{CB}}$, where red corresponds to the highest $\hat{\phi}_{\text{CB}}$ values and purple to the lowest $\hat{\phi}_{\text{CB}}$ values. The top five panels are measured at shear rates where $Bi^{-1} < 1$ and the bottom five panels at shear rates where $Bi^{-1} > 1$.

to homogenize the suspension. These measurements show that the growth and densification of agglomerates gives rise to sedimentation, which results in an apparent thinning of the suspension with increased shear time. Further, the data at $Bi^{-1} > 1$ show that heterogeneities can be reversibly eliminated via the preshear of 2500 s^{-1} .

IV. DISCUSSION

The observations presented here show that two distinct trajectories in both the macroscopic properties and the microstructure of sheared carbon black suspensions can be demarcated using the inverse Bingham number, $Bi^{-1} = \sigma/\sigma_y$. For $Bi^{-1} > 1$, open, branched agglomerates undergo a self-similar breakdown with increasing shear rate. This microstructural behavior is reflected in a reversible shear-thinning behavior as well as a stable volume fraction distribution along the height of the Couette. For $Bi^{-1} < 1$, shearing results in the growth and densification of agglomerates. This results in a rheopectic behavior where a decrease in the hydrodynamic volume fraction dictates a decrease in the apparent viscosity. During this restructuring process, inter-agglomerate bonds are exchanged for intra-agglomerate bonds, resulting in a weaker, more fragile gel whose elastic properties are dependent on the degree of restructuring. This weakened network, along with the increased size and density of the agglomerates, cause a long-lived apparent stress response that arises due to sedimentation.

Sedimentation of particles in suspension has been observed previously for non-Brownian suspensions as well as aggregating colloidal suspensions [58–61]. Acrivos *et al.* have shown that for non-Brownian suspensions, a balance between shear-induced diffusivity and sedimentation exists so that the onset of sedimentation is predictable by the order of magnitude of a modified Shields' parameter, A , which relates viscous forces to gravitational forces [58]. In this model, when A is of order of magnitude greater than 1, viscous forces dominate and the particles should resuspend or remain suspended under shear, and when A is of order of

magnitude less than 1, gravitational forces dominate and the suspension is expected to sediment under shear. The Shields' parameter can be calculated for the suspension studied here and can be used as a rule of thumb for predicting whether or not sedimentation will occur. As shown in Eq. (3), this parameter depends on the viscosity of the suspending medium, η_m , the density difference between the two phases in the suspension, $\Delta\rho = \rho_{\text{particle}} - \rho_{\text{medium}}$, the shear rate, $\dot{\gamma}$, the gravitational constant, g , and the original thickness of the resuspension layer, h_0 [58].

$$A = \frac{9}{2} \frac{\eta_m \dot{\gamma}}{h_0 g \Delta\rho}. \quad (3)$$

An estimate of Shields' parameter can be made for the structures formed at $Bi^{-1} > 1$ and $Bi^{-1} < 1$. For the original thickness of the resuspension layer, h_0 , the height of the Couette in the Rheo-SANS experiments is used so that $h_0 = 36 \text{ mm}$. From this estimate, the shear rate, $\dot{\gamma}$, is set as the shear rates bounding the two flow regimes, which are 500 s^{-1} and 400 s^{-1} for $Bi^{-1} > 1$ and $Bi^{-1} < 1$, respectively. To determine the density of the agglomerates, ρ_{particle} , a fractal dimension, D_f , and radius of gyration, R_g , is estimated for both flow regimes. The open structures formed for $Bi^{-1} > 1$ are assumed to have a fractal dimension of $D_f = 1.9$ and a radius of gyration of $R_g = 2 \mu\text{m}$. These values come from results shown in Fig. 6. The agglomerates formed for $Bi^{-1} < 1$ are outside of the size range measurable in uSANS ($15 \mu\text{m}$ or larger) and are more compact than the structures formed for $Bi^{-1} > 1$. For the purpose of this estimation, the agglomerates formed for $Bi^{-1} < 1$ are assumed to have a radius of gyration of $R_g = 15 \mu\text{m}$ and a fractal dimension of $D_f = 2.5$. While this estimation of the radius of gyration is a lower bound one based on the resolution of uSANS, the order of magnitude of A remains the same for values of R_g up to the size of the gap (0.5 mm). The value for the fractal dimension used is reasonable and has been previously reported by Rueb and Zukoski for a sheared suspension of octadecyl silica particles [16].

The radius of the gyration and fractal dimension are used to calculate the volume fraction of carbon black in the internal volume of an agglomerate, $\varphi_{CB, Ragg}$, as described in Richards *et al.* [27]. Due to the porosity of the primary particles comprising the agglomerates [27] as well as their fractal nature, $\varphi_{CB, Ragg}$ is small and less than 0.1 in both flow regimes. The calculated $\varphi_{CB, Ragg}$ is used to calculate the density of an agglomerate, $\rho_{particle}$. Using these parameters, the Shields' parameter is of the order of magnitude 1 for $Bi^{-1} < 1$ and of the order of magnitude 10 for $Bi^{-1} > 1$. Although this calculation does not account for the effect of hydrodynamic interactions [62], it provides a valuable understanding of our experimental results, where vertical concentration gradients are observed for $Bi^{-1} < 1$ and a homogeneous suspension is observed for $Bi^{-1} > 1$.

The initial decay in stress observed upon flow start-up at all shear rates logically suggests a time-dependent microstructural transformation. Therefore, both the applied shear rate and the time allowed for restructuring plays an important role in the apparent macroscopic properties of the suspension. For $Bi^{-1} < 1$, this restructuring time is convoluted with the continuous sedimentation that occurs over the entire shear time. To determine the relative importance that the shear-induced microstructure and sedimentation have on the apparent macroscopic properties, $\hat{\varphi}_{CB}$ values are averaged over the measurable Couette height and Bi^{-1} are plotted against the applied shear rate in Figs. 10(b) and 10(a), respectively, for different times throughout the Rheo-SANS test. Both Bi^{-1}

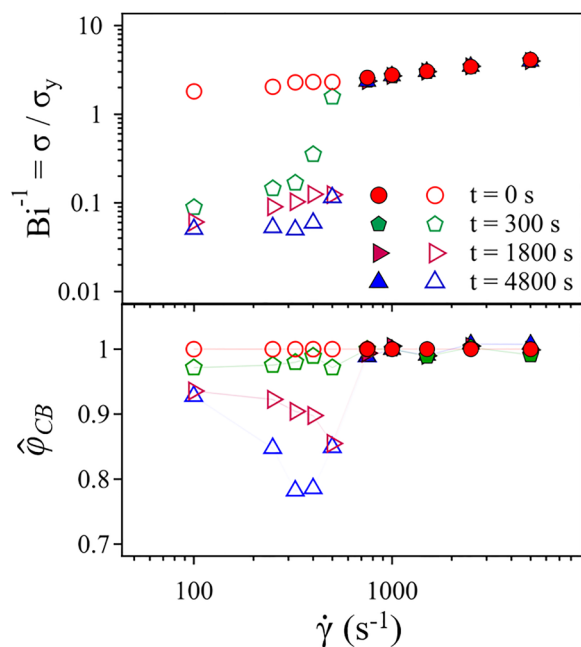


FIG. 10. Summary of results from a Rheo-SANS experiment on a suspension of Vulcan XC-72 carbon black in propylene carbonate with $\varphi_{eff} = 0.274$. (a) Apparent flow curves plotted as inverse Bingham number against shear rate measured at different times where open symbols represent $Bi^{-1} < 1$ and closed symbols represent $Bi^{-1} > 1$. The value at $t = 0$ s (red circles) was obtained by extrapolating the time-dependent stress response using an exponential fit. Other flow curves were taken at $t = 300$ s (green pentagons), $t = 1800$ s (pink triangles), and at the final time of $t = 4800$ s (blue triangles). (b) Different time points of $\hat{\varphi}_{CB}$ averaged over all measurable Couette heights plotted against the applied shear rate.

and $\hat{\varphi}_{CB}$ remain nearly constant at shear rates where $Bi^{-1} > 1$. For $Bi^{-1} < 1$, however, the effect of the growth and densification is clear. For the initial 300 s, the apparent stress decreases significantly, but the averaged $\hat{\varphi}_{CB}$ over all measurable heights, here a proxy for the extent of sedimentation, remains nearly constant. This implies that the restructuring of agglomerates is the main contributor to this large decrease in the apparent stress at early times. At longer times, sedimentation occurs. At these times, the reduction in $\hat{\varphi}_{CB}$ averaged over the middle half of the Couette geometry generally corresponds with the further decrease in apparent stress. From this, it is evident that the agglomerates first go through a microstructural transformation and then begin to settle as a result of this transformation.

It is important to note that this behavior may be present in other suspensions that display long-range attractions between particles that lead to a large-scale structure formation. This can become a complicating factor in applications that require long periods of flow and in measurements aimed at probing the shear-dependent properties of a suspension. For parallel plate and cone and plate geometries, the volume fraction may not be evenly distributed across the gap, resulting in a measured response that does not accurately represent the bulk material behavior. Furthermore, for Couette geometries, a significant amount of the solid fraction will progressively migrate to the bottom of the geometry so that the actual volume fraction being measured is variable.

The measured shear-induced microstructural evolution of this suspension of carbon black in propylene carbonate provides an understanding of observations that have previously been made in the literature concerning the complex rheological behavior of carbon black suspensions. Our measurements show that for $Bi^{-1} < 1$, the two transient behaviors observed in the stress and conductivity arise due to the densification of agglomerates and resulting sedimentation. This densification process has been observed previously by Osuji *et al.* for carbon black suspended in tetradecane [35] and is a common explanation for the shear-dependent macroscopic properties of carbon black suspended in a variety of media. Our results confirm this observation and show that sedimentation gives rise to additional geometry-dependent complexities.

Tunability of macroscopic properties such as the yield stress and conductivity are commonly observed in carbon black suspensions [28,29] and are consistent with the exchange of inter-agglomerate bonds for intra-agglomerate bonds via densification upon transitioning from $Bi^{-1} > 1$ to $Bi^{-1} < 1$. This exchange results in a decrease in the degree of jamming with a decrease in shear rate where a weaker network is achieved after shearing at low shear intensities as illustrated in Fig. 11. Additionally, due to the sedimentation that arises from this structural densification, it can be expected that shearing for longer times at a shear rate where $Bi^{-1} < 1$ will result in a progressively lower yield stress and conductivity. Furthermore, the apparent shear-thickening behavior shown in Fig. 3(c) and observed by Osuji *et al.* [35] and Narayanan *et al.* [34] is directly identified as resulting from the erosion of densified agglomerates and the capture of propylene carbonate into the internal agglomerate structure (Fig. 11) when the stress exceeds the macroscopic yield

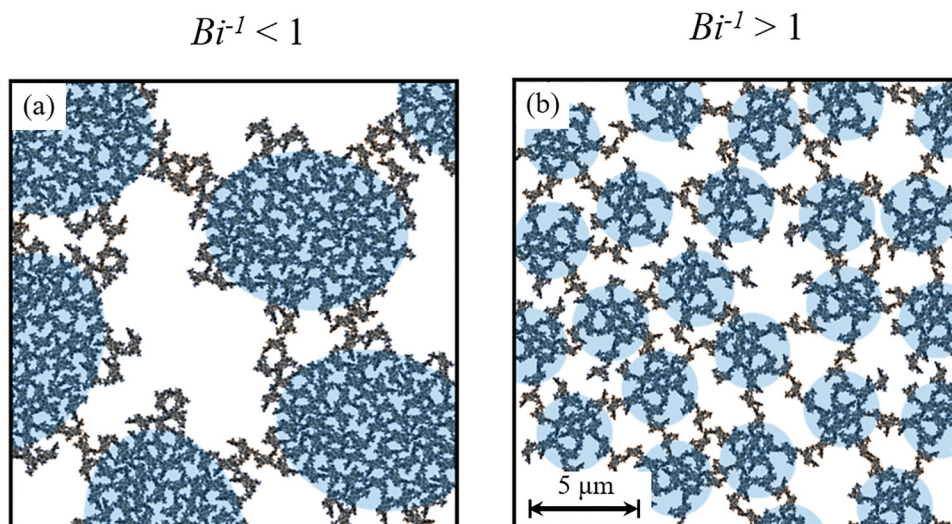


FIG. 11. Illustration of the two structural categories achieved under shear. Each blue shaded circle represents one carbon black agglomerate comprised of many primary aggregates. (a) The loosely connected network with large amounts of free solvent comprised of the large, dense agglomerates formed at $Bi^{-1} < 1$ and (b) the strongly connected network comprised of the small, open agglomerates formed at $Bi^{-1} > 1$.

stress. Due to sedimentation, this apparent shear-thickening transition becomes more severe with increasing shear time, as is seen in Fig. 3(c). Our experiments measuring rheology, conductivity, and microstructure show that the “true” yield stress of the presheared suspension marks the boundary between two microstructural and macroscopic trajectories under shear flow. The first, for $Bi^{-1} > 1$, is characterized by classical reversible thixotropy where the agglomerates restructure due to the imposed hydrodynamic stress of the flow. The second, for $Bi^{-1} < 1$, is identified by the densification of agglomerates due to a balance of the shear stress and developing elasticity of the network. This latter flow region is heterogeneous and subject to sedimentation during flow. By using a dimensionless group that takes into account the yield stress of the presheared suspension, this behavior is expected to hold more broadly for suspensions of carbon black in a variety of media where factors such as interparticle interactions, density mismatch, and shear history are subject to change.

V. CONCLUSIONS

Rheo-uSANS and spatiotemporally resolved Rheo-SANS measurements have been used to identify two shear-induced microstructural trajectories for the suspension of carbon black in propylene carbonate that explain the complex, shear-history dependent rheology previously reported for this class of dispersions. We show that the bifurcation of these two rheological behaviors are demarcated by the inverse Bingham number, $Bi^{-1} = \sigma/\sigma_y$, which determines the transient nature of the suspension under shear. For $Bi^{-1} > 1$, open, relatively small agglomerates are formed and the suspension remains homogeneous under quasisteady conditions. In contrast, for $Bi^{-1} < 1$, a shear-driven transformation from these small, but open agglomerates to large, denser agglomerates results in a steep decrease in both the apparent viscosity and conductivity, which continue to decline with shear time due to complicating effects of sedimentation. The decrease in

hydrodynamic volume fraction associated with this microstructural evolution was shown to have a more significant effect on the macroscopic properties than the slow migration of carbon black associated with sedimentation. The measured transient microstructural behavior and resulting change in macroscopic properties have implications for applications where processing or end-use require extended flow periods. This microstructural characterization helps to explain many observations in the literature regarding carbon black suspensions including tunability of the yield stress and elasticity, an apparent shear-thickening behavior, and transient macroscopic properties.

ACKNOWLEDGMENTS

The authors acknowledge the NIST Center for Neutron Research CNS Cooperative Agreement No. 70NANB12H239 grant for partial funding and the National Research Council for support. Access to the NG3 vSANS instrument and BT5 uSANS instrument was provided by the Center for High Resolution Neutron Scattering, a partnership between the National Institute of Standards and Technology and the National Science Foundation under Agreement No. DMR-1508249. The authors also acknowledge the support of the National Institute of Standards and Technology, U.S. Department of Commerce, in providing the neutron research facilities used in this work. This work benefited from the use of the SASVIEW application, originally developed under NSF Award No. DMR-0520547. SASVIEW also contains code developed with funding from the EU Horizon 2020 program under the SINE2020 Project Grant No. 654000. Certain commercial equipment, instruments, or materials are identified in this paper to foster understanding. Such identification does not imply recommendation or endorsement by the National Institute of Standards and Technology nor does it imply that the materials or equipment identified are necessarily the best available for the purpose.

REFERENCES

- [1] Weir, A., L. Westerhoff, K. Hristovski, and N. von Goetz, "Titanium dioxide nanoparticles in food and personal care products," *Environ. Sci. Technol.* **46**, 2242–2250 (2012).
- [2] Hellinckx, L., and J. Mewis, "Rheological behaviour of pigment dispersions as related to roller passage," *Rheol. Acta* **8**, 519–525 (1969).
- [3] Feys, D., R. Verhoeven, and G. De Schutter, "Why is fresh self-compacting concrete shear thickening?," *Cem. Concr. Res.* **39**, 510–523 (2009).
- [4] Russel, W. B., "Review of the role of colloidal forces in the rheology of suspensions," *J. Rheol.* **24**, 287–317 (1980).
- [5] Trappe, V., and D. A. Weitz, "Scaling of the viscoelasticity of weakly attractive particles," *Phys. Rev. Lett.* **85** (2), 449–452 (2000).
- [6] Eberle, A. P. R., J. M. Kim, and N. J. Wagner, "Dynamical arrest, percolation, gelation, and glass formation in model nanoparticle dispersions with thermoreversible adhesive interactions," *Langmuir* **28**, 1866–1878 (2012).
- [7] Lekkerkerker, H. N. W., W. C. K. Poon, P. N. Pusey, A. Stroobants, and P. B. Warren, "Phase behaviour of colloid + polymer mixtures," *Europhys. Lett.* **20** (6), 559–564 (1992).
- [8] Mewis, J., and N. J. Wagner, *Colloidal Suspension Rheology* (Cambridge University, Cambridge, 2012).
- [9] Varadan, P., and M. J. Solomon, "Shear-induced microstructural evolution of a thermoreversible colloidal gel," *Langmuir* **17**, 2918–2929 (2001).
- [10] Vermant, J., and M. J. Solomon, "Flow-induced structure in colloidal suspensions," *J. Phys. Condens. Matter* **17**, R187–R216 (2005).
- [11] Wessel, R., and R. C. Ball, "Fractal aggregates and gels in shear flow," *Phys. Rev. A* **46**, 3008–3011 (1992).
- [12] Pignon, F., A. Magnin, and J. Piau, "Thixotropic behavior of clay dispersions : Combinations of scattering and rheometric techniques," *J. Rheol.* **42**, 1349–1373 (1998).
- [13] Tolpekin, V. A., M. H. G. Duits, D. Van Den Ende, and J. Mellema, "Aggregation and breakup of colloidal particle aggregates in shear flow, studied with video microscopy," *Langmuir* **20**, 2614–2627 (2004).
- [14] Eggensdorfer, M. L., D. Kadau, H. J. Herrmann, and S. E. Pratsinis, "Fragmentation and restructuring of soft-agglomerates under shear," *J. Colloid Interface Sci.* **342**, 261–268 (2010).
- [15] Sonntag, R. C., and W. B. Russel, "Structure and breakup of flocs subjected to fluid stresses I. Shear experiments," *J. Colloid Interface Sci.* **113** (2), 399–413 (1986).
- [16] Rueb, C. J., and C. F. Zukoski, "Viscoelastic properties of colloidal gels," *J. Rheol.* **41**, 197–218 (1997).
- [17] Hoekstra, H., J. Vermant, J. Mewis, and G. G. Fuller, "Flow-induced anisotropy and reversible aggregation in two-dimensional suspensions," *Langmuir* **19**, 9134–9141 (2003).
- [18] Verduin, H., B. J. De Gans, and J. K. G. Dhont, "Shear induced structural changes in a gel-forming suspension studied by light scattering and rheology," *Langmuir* **12**, 2947–2955 (1996).
- [19] Osuji, C. O., and D. A. Weitz, "Highly anisotropic vorticity aligned structures in a shear thickening attractive colloidal system," *Soft Matter* **4**, 1388–1392 (2008).
- [20] Grenard, V., N. Taberlet, and S. Manneville, "Shear-induced structuration of confined carbon black gels: Steady-state features of vorticity aligned flocs," *Soft Matter* **7**, 3920–3928 (2011).
- [21] Eberle, A. P. R., N. Martys, L. Porcar, S. R. Kline, W. L. George, J. M. Kim, P. D. Butler, and N. J. Wagner, "Shear viscosity and structural scalings in model adhesive hard-sphere gels," *Phys. Rev. E* **89**, 050302 (2014).
- [22] Kim, J. M., A. P. R. Eberle, A. K. Gurnon, L. Porcar, and N. J. Wagner, "The microstructure and rheology of a model, thixotropic nanoparticle gel under steady shear and large amplitude oscillatory shear (LAOS)," *J. Rheol.* **58**, 1301–1328 (2014).
- [23] Donnet, J. B., "Nano and microcomposites of polymers elastomers and their reinforcement," *Compos. Sci. Technol.* **63**, 1085–1088 (2003).
- [24] Donnet, J. B., R. C. Bansal, and M. J. Wang, *Carbon Black Science and Technology*, 2nd ed. (Marcel Dekker, New York, 1993).
- [25] Spinelli, H. J., "Polymeric dispersants in ink jet technology," *Adv. Mater.* **10** (15), 1215–1218 (1998).
- [26] Duduta, M., B. Ho, V. C. Wood, P. Limthongkul, V. E. Brunini, W. C. Carter, and Y. Chiang, "Semi-solid lithium rechargeable flow battery," *Adv. Energy Mater.* **1**, 511–516 (2011).
- [27] Richards, J. J., J. B. Hipp, J. K. Riley, N. J. Wagner, and P. D. Butler, "Clustering and percolation in suspensions of carbon black," *Langmuir* **33** (43), 12260–12266 (2017).
- [28] Ovarlez, G., L. Tocquer, F. Bertrand, and P. Coussot, "Rheopexy and tunable yield stress of carbon black suspensions," *Soft Matter* **9**, 5540–5549 (2013).
- [29] Helal, A., T. Divoux, and G. H. McKinley, "Simultaneous rheo-electric measurements of strongly conductive complex fluids," *Phys. Rev. Appl.* **6**, 64004 (2016).
- [30] Mewis, J., and N. J. Wagner, "Thixotropy," *Adv. Colloid Interface Sci.* **147-148**, 214–227 (2009).
- [31] Armstrong, M. J., A. N. Beris, S. A. Rogers, and N. J. Wagner, "Dynamic shear rheology and structure kinetics modeling of a thixotropic carbon black suspension," *Rheol. Acta* **56**, 811–824 (2017).
- [32] Dullaert, K., and J. Mewis, "Thixotropy: Build-up and breakdown curves during flow," *J. Rheol.* **49**, 1213–1230 (2005).
- [33] Negi, A. S., and C. O. Osuji, "New insights on fumed colloidal rheology—Shear thickening and vorticity-aligned structures in flocculating dispersions," *Rheol. Acta* **48**, 871–881 (2009).
- [34] Narayanan, A., F. Mugele, and M. H. G. Duits, "Mechanical history dependence in carbon black suspensions for flow batteries: A rheo-impedance study," *Langmuir* **33**, 1629–1638 (2017).
- [35] Osuji, C. O., C. Kim, and D. A. Weitz, "Shear thickening and scaling of the elastic modulus in a fractal colloidal system with attractive interactions," *Phys. Rev. E* **77**, 60402 (2008).
- [36] Dagastine, R. R., D. C. Prieve, and L. R. White, "Calculations of van der Waals forces in 2-dimensionally anisotropic materials and its application to carbon black," *J. Colloid Interface Sci.* **249**, 78–83 (2002).
- [37] Dullaert, K., and J. Mewis, "Stress jumps on weakly flocculated dispersions: Steady state and transient results," *J. Colloid Interface Sci.* **287**, 542–551 (2005).
- [38] Barnes, H. A., "The yield stress—a review or 'panta roi'—everything flows?," *J. Nonnewton. Fluid Mech.* **81**, 133–178 (1999).
- [39] Perge, C., N. Taberlet, T. Gibaud, and S. Manneville, "Time dependence in large amplitude oscillatory shear: A rheo-ultrasonic study of fatigue dynamics in a colloidal gel," *J. Rheol.* **58**, 1331–1357 (2014).
- [40] Richards, J. J., N. J. Wagner, and P. D. Butler, "A strain-controlled RheoSANS instrument for the measurement of the microstructural, electrical, and mechanical properties of soft materials," *Rev. Sci. Instrum.* **88** (10), 105115 (2017).
- [41] Richards, J. J., C. V. L. Gagnon, J. R. Krzywon, N. J. Wagner, and P. D. Butler, "Dielectric RheoSANS—Simultaneous interrogation of impedance, rheology and small angle neutron scattering of complex fluids," *J. Vis. Exp.* **122**, e55318 (2017).
- [42] Barker, J. G., C. J. Glinka, J. J. Moyer, M. H. Kim, A. R. Drews, and M. Agamalian, "Design and performance of a thermal-neutron double-crystal diffractometer for USANS at NIST research papers," *J. Appl. Crystallogr.* **38**, 1004–1011 (2005).

- [43] Porcar, L., D. Pozzo, G. Langenbacher, J. Moyer, and P. D. Butler, "Rheo—small-angle neutron scattering at the national institute of standards and technology center for neutron research," *Rev. Sci. Instrum.* **82**, 1–8 (2011).
- [44] Eberle, A. P. R., and L. Porcar, "Flow-SANS and rheo-SANS applied to soft matter," *Curr. Opin. Colloid Interface Sci.* **17**, 33–43 (2012).
- [45] Kline, S. R., "Reduction and analysis of SANS and USANS data using IGOR Pro," *J. Appl. Crystallogr.* **39**, 895–900 (2006).
- [46] Kim, M., and C. J. Glinka, "Ultra small angle neutron scattering study of the nanometer to micrometer structure of porous Vycor," *Microporous Mesoporous Mater.* **91**, 305–311 (2006).
- [47] Kalman, D. P., and N. J. Wagner, "Microstructure of shear-thickening concentrated suspensions determined by flow-USANS," *Rheol. Acta* **48**, 897–908 (2009).
- [48] Beaucage, G., "Approximations leading to a unified exponential/power-law approach to small-angle scattering," *J. Appl. Crystallogr.* **28**, 717–728 (1995).
- [49] Beaucage, G., "Small-angle scattering from polymeric mass fractals of arbitrary mass-fractal dimension," *J. Appl. Crystallogr.* **29**, 134–146 (1996).
- [50] Doucet, M., J. H. Cho, G. Alina, J. Bakker, W. Bouwman, P. Butler, and A. Washington, SasView Version 4.1.2, Zenodo (12 Aug 2017).
- [51] Feigin, L. A., and D. I. Svergun, *Structure Analysis by Small-Angle X-ray and Neutron Scattering* (Plenum, New York, 1987).
- [52] Glatter, O., and O. Kratky, *Small Angle X-ray Scattering* (Academic, Cambridge, 1982).
- [53] Coussot, P., Q. D. Nguyen, H. T. Huynh, and D. Bonn, "Viscosity bifurcation in thixotropic, yielding fluids," *J. Rheol.* **46**, 573–589 (2002).
- [54] Mewis, J., L. M. De Groot, and J. A. Helsen, "Dielectric behaviour of flowing thixotropic suspensions," *Colloid Surf.* **22**, 249–269 (1987).
- [55] Amari, T., and K. Watanabe, "Flow properties and electrical conductivity of carbon black-linseed oil suspension," *J. Rheol.* **34**, 207–221 (1990).
- [56] Teixeira, J., "Small-angle scattering by fractal systems," *J. Appl. Crystallogr.* **21** (6), 781–785 (1988).
- [57] Koumakis, N., E. Moghimi, R. Besseling, W. C. K. Poon, J. F. Brady, and G. Petekidis, "Tuning colloidal gels by shear," *Soft Matter* **11**, 4640–4648 (2015).
- [58] Acrivos, A., X. Fan, and R. Mauri, "On the measurement of the relative viscosity of suspensions," *J. Rheol.* **38**, 1285–1296 (1994).
- [59] Buscall, R., "The sedimentation of concentrated colloidal suspensions," *Colloids and Surfaces* **43**, 33–53 (1990).
- [60] Davis, K. E., W. B. Russel, and W. J. Glantschnig, "Settling suspensions of colloidal silica: Observations and x-ray measurements," *J. Chem. Soc. Faraday Transl.* **87** (3), 411–424 (1991).
- [61] López-López, M. T., A. Zugaldía, F. González-Caballero, and J. D. G. Durán, "Sedimentation and redispersion phenomena in iron-based magnetorheological fluids," *J. Rheol.* **50**, 543–560 (2006).
- [62] Moncho-Jorda, A., A. A. Louis, and J. T. Padding, "Effects of interparticle attractions on colloidal sedimentation," *Phys. Rev. Lett.* **104**, 068301 (2010).
- [63] See supplementary material at <https://doi.org/10.1122/1.5071470> for information about the yield stress determination, alignment of the rheo-SANS Couette, and rheo-electric measurements and fitting of the Rheo-uSANS data.